Spatiomolecular Characterization of Dopamine D2 Receptors Cells in the Mouse External Globus Pallidus

Julie Espallergues, Jihane Boubaker-Vitre, Audrey Mignon, Maelle Avrillon, Morgane Le Bon-Jego, Jerome Baufreton, Emmanuel Valjent

▶ **To cite this version:**

Julie Espallergues, Jihane Boubaker-Vitre, Audrey Mignon, Maelle Avrillon, Morgane Le Bon-Jego, et al.. Spatiomolecular Characterization of Dopamine D2 Receptors Cells in the Mouse External Globus Pallidus. Current Neuropharmacology, In press, 10.2174/1570159X21666230720121027 . hal-04181821

HAL Id: hal-04181821
https://hal.science/hal-04181821

Submitted on 21 Aug 2023

HAL is a multi-disciplinary open access archive for the deposit and dissemination of scientific research documents, whether they are published or not. The documents may come from teaching and research institutions in France or abroad, or from public or private research centers.

L'archive ouverte pluridisciplinaire **HAL**, est destinée au dépôt et à la diffusion de documents scientifiques de niveau recherche, publiés ou non, émanant des établissements d'enseignement et de recherche français ou étrangers, des laboratoires publics ou privés.

Spatiomolecular characterization of dopamine D2 receptors cells in the mouse external globus pallidus

Julie Espallergues[1], Jihane Boubaker-Vitre[1], Audrey Mignon[1], Maelle Avrillon[1], Morgane Le Bon-Jego[2], Jerome Baufreton[2], Emmanuel Valjent[1]

[1] IGF, Univ. Montpellier, CNRS, Inserm, F-34094 Montpellier, France.

[2] Univ. Bordeaux, CNRS, IMN, UMR 5293, F-33000 Bordeaux, France.

Correspondence should be addressed to Emmanuel Valjent (E-mail: emmanuel.valjent@igf.cnrs.fr)

Keywords: dopamine, pallidostriatal, globus pallidus, cholinergic neurons.

Summary

The external globus pallidus (GPe) is part of the basal ganglia circuit and plays a key role in the control of actions. Although evidence indicate that dopamine through its activation of D2 receptors modulate the (D2Rs) GPe neural activity, the precise spatiomolecular characterization of cell populations expressing D2Rs in the mouse GPe is still lacking. By combining single molecule *in situ* hybridization, cell type-specific imaging analyses and electrophysiology slice recordings, we found that GPe D2R cells are neurons preferentially localized in the caudal portion of GPe. These neurons comprising pallidostriatal, pallidonigral and pallidocortical neurons segregate into two distinct populations displaying molecular and electrophygiological features of GPe GABAergic PV/NKX2.1 and cholinergic neurons respectively. By clarifying the spatial molecular identity of GPe D2R neurons in the mouse, this work provides basis for future studies aiming at disentangle action of dopamine within the GPe.

Introduction

The basal ganglia, comprising the striatum, the globus pallidus (GP), the subthalamic nucleus (STN) and the substancia nigra (SN), are part of an anatomical system involved in motor control, goal-directed behaviors and habit formation (1,2). More than a simple relay station, the external globus pallidus (GPe) serves as a key hub in the basal ganglia network (1). Indeed, GPe projection neurons integrate information from the two inputs nuclei of the basal ganglia, the striatum and STN and send processed information back to all basal ganglia nuclei, including the striatum, the internal GP (GPi), STN and SN, thereby optimizing the selection, initiation and execution of actions (1).

In rodents, most of GPe neurons are GABAergic projection neurons (~95%) complemented by cholinergic neurons (~5%) (2). GPe GABAergic neurons segregated into at least two distinct subpopulations, the prototypic and arkypallidal GPe neurons which can be identified by their electrophysiological and protein expression profiles, projections sites and functions (3-5). Because of the complete lack of interneurons within the GPe, the intrinsic regulation of information processing mainly relies on GABA released from collateral axons of GPe neurons (6,7) but is also achieved by various neuromodulators among which dopamine (8-10).

Early anatomical studies indicate that most of the midbrain dopamine neurons arising from the substancia pars compacta (SNc) and to a lesser extend from the ventral tegmental area (VTA) send collateral axons in the GPe (11-13). Moreover, converging evidence indicate that dopamine release can be evoked in the GPe (14) and that local intrapallidal dopamine release can profoundly modulate GPe neural activity (9,10,15). These effects are largely ascribed to the activation of dopamine D2 receptors (D2R) (9,16,17) found presynaptically at the striatopallidal terminals (18) and postsynaptically (19,20) in both parvalbumin-positive and -negative GPe neurons (21). However, all these evidence come from studies performed in rats

leaving open the question of the distribution, the molecular and electrophysiological identity of D2R-expressing cells in the mouse GPe neurons.

Here, we combined single molecule *in situ* hybridization, cell type-specific imaging analyses and electrophysiology to characterize D2R-expressing cells in the mouse GPe. Our analysis revealed that GPe D2R neurons are not evenly distributed along the rostro-caudal and dorso-ventral axis and indicate that GPe D2R neurons segregate in two subpopulations with distinct molecular and electrophysiological features.

Materials and methods

Animals

Male C57BL/6 (n = 3) from Charles River Laboratories, $Drd2^{Cre/+}$ (n = 4), $Drd2^{Cre/+}$;$Ai9^{f/+}$ (n = 6) and $Drd2^{Cre/+}$;$Ribotag^{f/+}$ (n = 29) were used in the present study. $Drd2^{Cre/+}$;$Ribotag^{f/+}$ mice were generated as previously described (22). Male 8- to 12-week old mice (25-30 gr) were used in the current study. All mice were housed in groups of 2 to 5 per cage (standard sizes according to the European animal welfare guidelines 2010/63/EU) and maintained in a 12h light/dark cycle (lights on from 7:00 am to 7:00 pm), in stable conditions of temperature (22°C) and humidity (60%), with food and water provided *ad libitum*. All animal procedures were conducted in accordance with the guidelines of the French Agriculture and Forestry Ministry for handling animals (authorization number/license B34-172-41) and approved by the relevant local and national ethics committees (authorizations APAFIS#14875 and APAFIS#14255).

Stereotaxic injection into the ventro-posterior GPe

Surgeries were performed on 8-10 weeks old $Drd2^{Cre/+}$;$Ribotag^{f/+}$ and $Drd2^{Cre/+}$ male mice. Animals were anesthetized with a mixture of ketamine (Imalgene 500, 50 mg/ml, Merial), 0.9% NaCl solution (weight/vol) and xylazine (Rompun 2%, 20 mg/ml, Bayer) (2:2:1, i.p., 0.1 ml/30 g) and mounted on a stereotaxic apparatus. The microinjection needle was connected to a 10 µl Hamilton syringe and filled with adeno-associated virus (AAV) containing ChR2-Td-Tomato, AAV2/1.CAGGS.flex.ChR2.tdTomato.SV40 (titer, 3.28E+12 GC/ml, Addgene #18917) (UPenn vector core, Philadelphia, USA) or AAV2/5.EF1a.DIO.eYFP (titer, 4E+12 GC/ml, Addgene #27056) (UNC vector core, Chapel Hill, USA). Microinjection needle was placed into the GPe (A/P = -1.5 mm; Lat. =2.5 mm; D/V = -3.75 mm) and 0.2 µl was injected over 5 min. The injector was left in place for an additional 5 min to allow for diffusion of virus particles

away from injection site. Wounds of mice were sealed by suture. Animals were then returned to their home cages for a 14 days recovery period.

Drugs and treatment

Quinpirole (1.0 mg/kg, i.p.) and raclopride (0.5 mg/kg) were purchased from Tocris and dissolved in 0.9% (w/v) NaCl (saline). Both drugs were administered at doses known to induce strong increased pS32-cFos expression (23,24). $Drd2^{Cre/+}$;$Ribotag^{f/+}$ mice were habituated to handling and saline injection three consecutive days before the experiment. Drugs were administrated on day 4. Mice were perfused as described below 90 min after injection.

Tissue preparation and immunofluorescence

Tissue preparation and immunofluorescence were performed as previously described ([25]). Mice were anaesthetized with Euthasol® (360 mg/kg, i.p., TVM lab, France) and transcardially perfused with 4% (weight/vol) paraformaldehyde in 0.1 M sodium phosphate buffer (pH 7.5). Brains were post-fixed overnight in the same solution and stored at 4°C. Brains were sliced (30-µm thick sections) with a vibratome (Leica, France) and stored at -20°C in a solution containing 30% (vol/vol) ethylene glycol, 30% (vol/vol) glycerol and 0.1 M sodium phosphate buffer (PBS), until they were processed for immunofluorescence (26). Coronal sections containing the ventro-posterior GPe were identified using a mouse brain atlas (27). The immunofluorescence was performed as follow: *day 1*, free-floating sections were a) rinsed three times 10 min in PBS, b) incubated 15 min in 0.1% (vol/vol) Triton X-100 in PBS, c) rinsed again three times 10 min in PBS, d) blocked for 1 h in a solution of 3% BSA in PBS and e) incubated 72 hours at 4°C with the primary antibodies (Supplemental Table 1) diluted in a PBS solution containing 1% BSA and 0.15% Triton X-100; *day 2*, sections a) were rinsed three times for 10 min in PBS, b) incubated for 45 min with secondary antibodies with goat Cy2-, Cy3- and

Cy5-coupled (1:400, Jackson Immunoresearch) and/or goat alexafluor 488 (1:400, Life Technologies) secondary antibodies and c) rinsed for 10 minutes (twice) in PBS before mounting in DPX (Sigma-Aldrich, Saint-Quentin Fallavier, France). Confocal microscopy was carried out at the Montpellier RIO Imaging Facility. Images covering the rostro-caudal extension of the GPe were sections acquired using NanoZoomer (Hamamatsu). Double-immunolabeled images were single confocal sections acquired using sequential laser scanning confocal microscopy (Leica SP8). HA -positive cells were pseudocolored in green while other markers were pseudocolored in red. All parameters were held constant for all sections from the same experiment. Images used for quantification were all single confocal sections. HA-positive cells were manually counted in the ventro-posterior GPe (from bregma -1.00 to -1.56 mm). Adjacent serial sections were never counted for the same marker to avoid any potential double counting of hemisected neurons. Values in the histograms in Figure 1 represent an estimated percentage of HA-positive neurons in throughout the rostro-caudal extension of the GPe (16 hemispheres per mouse, n = 4 mice). Values in the histograms in Figure 4-6 and S3 represent the co-expression as percentage of HA-positive neurons (green) and as percentage of cells expressing the different markers tested (red) (7-10 hemispheres per mouse, n = 6 mice). Total numbers of HA- and marker-positive cells counted are indicated between parentheses.

Single molecule fluorescent *in situ* hybridization

Analyses of *Drd2*, *Pvalb*, *Penk*, *Chat* and *Slc18a3* mRNAs expression were performed using single molecule fluorescent *in situ* hybridization (smFISH) (28). Brains from 3 C57BL/6 male mice were rapidly extracted and snap-frozen on dry ice and stored at -80°C until use. Sixteen µm coronal sections of the PAG (bregma -4.60 mm) were collected directly onto Superfrost Plus slides (Fisherbrand). Coronal sections were collected from bregma -1.00 mm to -1.56 mm. Probes for *Drd2* (ACDBio; Mm-drd2-C3, Cat# 406501-C3), *Pvalb* (ACDBio; Mm-pvalb-C2,

Cat# 421931-C2), *Penk* (ACDBio; Mm-penk-C1, Cat# 318761), *Chat* (ACDBio; Mm-chat-C1, Cat# 408731) and *Slc18a3* (ACDBio; Mm-slc18a3-C1, Cat# 448771) were used with the RNAscope Fluorescent Multiplex Kit (ACDBio; Cat# 320850) according to manufacturer's recommendations. After incubation with fluorescent-labeled probes, slides were counterstained with DAPI and mounted with ProLong Diamond Antifade mounting medium (Thermo Fisher scientific P36961). Confocal microscopy and image analyses were carried out at the Montpellier RIO imaging facility. Double- and triple-labeled images from the region of interest were single confocal sections captured using sequential laser scanning confocal microscopy (Leica SP8). Values in the histograms represent co-expression as percentage of *Drd2*-expressing cells (green) and as percentage of cells expressing the other markers tested (*Pvalb, Chat*, *Penk* and *Slc18a3*) (3-4 images in the GPe per mouse, n = 3 mice).

Ex vivo electrophysiology

Slice preparation. Brain slices containing the GPe were prepared as previously described (29). Briefly, $Drd2^{Cre/+}$ or $Drd2^{Cre/+}$;$Ai9^{f/+}$ mice were deeply anaesthetized with a mixture of ketamine/xylazine (100 mg/kg and 20 mg/kg, respectively). Then a thoracotomy was performed to allow transcardial perfusion of a saturated (Carbogen: 95% O2/5% CO2) iced-cold modified ACSF (cutting solution) composed of (in mM) 250 mM sucrose, 10 mM $MgSO_4 \cdot 7H_2O$, 2.5 mM KCl, 1.25 mM $NaH_2PO_4 \cdot H_2O$, 0.5 mM $CaCl_2 \cdot H_2O$, 1.3 mM $MgCl_2$, 26 mM $NaHCO_3$, and 10 mM D-glucose. After decapitation, the brain was quickly removed, glued on the stage of a vibratome (VT1200S, Leica microsystems), immerged in saturated iced-cold cutting solution and cut into coronal (300-µm thick) sections. Slices were then incubated at 34°C for 1 h in a standard ACSF saturated by bubbling carbogen and containing 126 mM NaCl, 2.5 mM KCl, 1.25 mM $NaH_2PO_4 \cdot H_2O$, 2 mM $CaCl_2 \cdot H_2O$, 2 mM $MgSO_4 \cdot 7H_2O$, 26 mM $NaHCO_3$, and 10

mM D-glucose, supplemented with 5 mM glutathion and 1 mM sodium pyruvate. They were maintained at room temperature in the same solution until recording.

Electrophysiology. Whole-cell patch-clamp experiments were performed in a submersion recording chamber under an upright microscope (Ni-E workstation, Nikon). Slices were bathed in ACSF containing 126 mM NaCl, 3 mM KCl, 1.25 mM $NaH_2PO_4 \cdot H_2O$, 1.6 mM $CaCl_2 \cdot H_2O$, 2 mM $MgSO_4 \cdot 7H_2O$, 26 mM $NaHCO_3$, and 10 mM D-glucose (pH: 7.4; Osmolarity: 310-315 mOsm). Caudal GPe neurons were visualized with infrared differential interference contrast and fluorescence microscopy (Spectra X light engine, Lumencor). D2R-positive GPe cells were identified either by the fluorescence of eYFP or tdTomato depending on the mouse line used for the experiment. Recording pipettes (5-7 MΩ) were prepared from borosilicate glass capillaries (GC150F-10; Harvard Apparatus) with a horizontal puller (Sutter Instrument, Model P-97). They were filled with an internal solution composed of 135 mM K-gluconate, 3.8 mM NaCl, 1 mM $MgCl_2 \cdot 6H_2O$, 10 mM HEPES, 0.1 mM Na_4EGTA, 0.4 mM Na_2GTP, and 2 mM $Mg_{1.5}$ATP (pH: 7.25; Osmolarity: 290-295 mOsm). Experiments were conducted using a Multiclamp 700B amplifier and Digidata 1440 digitizer controlled by Clampex 10.3 (Molecular Devices) at 34°C. Data were acquired at 20 kHz and low-pass filtered at 4 kHz. Whole-cell patch clamp recordings were not corrected for junction potential which was of 13mV with K-gluconate-based solution. All the recordings were performed in current-clamp mode and in the presence of ionotropic glutamatergic and GABAergic receptor blockers. NMDA receptors were inhibited by 50 µM D-(-)_2-amino-5-phosphonopentanoic acid (APV), AMPA/kainate receptors by 20 µM 6,7-dinitroquinoxaline- 2,3-dione (DNQX) and $GABA_A$ receptors by 10 µM GABAzine (SR95531). Intrinsic properties of the recorded neurons were investigated using increasing current pulse injections (50 pA steps, ranging from -100 to 250 pA, 1000 ms duration). Chemicals and pharmacologic compounds were purchased from Sigma-Aldrich and Tocris, respectively.

Analyses and statistics. Neuronal intrinsic properties analyses were performed with Clampfit 10.3 and Origin 7. Principal component (PCA) and dendrogram analyses were performed using Prism 9 (GraphPad Software) and the XLSTAT plug-in of excel software. Statistical analysis was performed with Prism 9 (GraphPad Software). Population data are presented as mean ± SEM. Unpaired data were compared using the Mann-Whitney U test (MW-U) test. Comparisons of F-I relationships were performed with a two-way repeated-measures ANOVA test followed by a Bonferroni test for multiple comparisons. Data were considered statistically significant for p values < at 0.05 (* $p < 0.05$; n.s., not significant).

Results

Distribution of GPe D2R neurons along the rostro-caudal and dorso-ventral axis

Although early *in situ* hybridization studies revealed the presence of *Drd2* transcripts in the GPe (30), information regarding the distribution of D2R cells throughout the external globus pallidus (GPe) rostro-caudal axis are still lacking. Because dense GFP-labeled striatopallidal terminals detected in $Drd2^{eGFP/+}$ mice preclude the identification of GPe D2R neurons (31,32), we bred mice harboring the $Drd2^{Cre/+}$ and the $Ribotag^{f/f}$ (33) reporter allele expressing the ribosomal protein Rpl22 tagged with the hemagglutinin (HA) epitope in a Cre-dependent manner ($Drd2^{Cre/+}$;$Ribotag^{f/+}$ mice) (25). The detection of HA immunoreactivity using anti-HA antibody revealed that GPe D2R cells found in the vicinity of TH-positive fibers (**Supplemental Figure 1**) were neurons and not microglia or glial cells as indicated by the lack of co-localization of HA with Iba1 and GFAP (**Supplemental Figure 2a-b**). Our analysis of anteroposterior and dorso-ventral sections revealed that GPe D2R neurons were not randomly distributed (**Figure 1a-b**). Indeed, the density of HA-positive gradually increased throughout the rostro-caudal axis being more concentrated in the ventro-posterior GPe (**Figure 1a-c**).

D2R neurons located in the ventro-posterior GPe project to distinct brain areas

We then used an anterograde tracing strategy to identity the ventro-posterior GPe D2R neurons projecting areas (**Figure 2a**). We first expressed mCherry selectively in GPe D2R neurons of $Drd2^{Cre/+}$;$Ribotag^{f/+}$ mice to confirm that mCherry-labelled cells were found in HA-positive cells. As shown in Figure 2, local injection into the caudal GPe triggered expression of mCherry in HA-positive cells ruling out the possibility that the expression pattern of HA reflect the developmental cumulative expression history of the reporter gene (**Figure 2b**).

We then searched for areas containing visible mCherry-labeled axons in the whole brain. Dense labelling was identified in several brain areas including the tail of the striatum (TS), the

posterior intralaminar nucleus (PIL), the ventral part of the SN *pars reticulata* (SNr), the auditory cortex (AC), and the ectorhinal and temporal association cortices (TeA, Ect) (**Figure 2c**). The diversity of areas identified suggest that ventro-posterior GPe D2R neurons are composed of segregated neural populations comprising at least pallidostriatal, pallidonigral and pallidocortical neurons. The absence of detectable fibers in the STN also suggests a weak overlap between GPe D2R and STN-projecting GPe neurons.

Electrophysiological signatures of D2R neurons located in the ventro-posterior GPe

We then looked for the characterization of the electrophysiological signatures of D2R GPe neurons using patch-clamp recordings in coronal brain slices obtained from $Drd2^{Cre/+}$ mice transfected with an AAV-EF1a-DIO-eYFP (**Figure 3a**) or $Drd2^{Cre/+}$;$Ai9^{f/+}$ mice. To define the electrophysiological profile of these neurons, eYFP- or tdTomato-positive neurons were recorded in presence in the ACSF of GABAergic and glutamatergic synaptic transmission blocker (GABAzine, 10 µM; DNQX, 20 µM and APV, 50 µM). 27 neurons located in the caudal portion of the GPe (**Figure 3b**) were recorded in current-clamp mode and several parameters such as resting membrane potential, spontaneous firing rate, driven firing rate, sag amplitude or firing frequency accommodation were collected from each cell. Principal component analysis performed on all these parameters revealed the existence of two distinct cell types within D2R GPe neurons according to their electrophysiological signature (**Figure 3c-d**). Type I neurons (n = 13) were characterized by their higher spontaneous firing rate (**Figure 3e-f**), the presence of stronger sag (**Figure 3h-j**) and the capacity to fire at higher frequencies upon current injections (**Figure 3k**)compared to type II neurons (n = 14). These electrophysiological signatures were pretty similar with the properties of choline acetyltransferase (ChAT)-positive and ChAT-negative pallidocortical GPe neurons described previously (34).

D2R neurons located in the ventro-posterior GPe are molecularly distinct

GABAergic neurons account for about 95% of the GPe neurons (1). These neurons fall into two molecularly distinct intermingled neuronal population identified by the expression of *Pvalb/Nkx2.1* and *Foxp2/Penk* transcripts, respectively (3,4). We therefore examined the relationship between these two populations and GPe D2R neurons. Using single molecule fluorescent *in situ* hybridization (smFISH), we found that ~50% of *Drd2*-positive cells of the ventro-posterior GPe were *Pvalb* (**Figure 4a-b**). Similar proportion was observed when the percentage of immunofluorescence HA positive neurons co-expressing parvalbumin (PV) was analyzed (**Figure 4c-d**). Consistent with the compartmentalization of PV-positive neurons in CB-lacking zones, less than 1% HA-expressing neurons were calbindin-28kD (CB) positive cells (**Supplemental Figure 3a-b**) (35). We also found that a majority of HA-immunoreactive expressed the transcription factor NKX2.1 (~94.6%) (**Figure 4e-f**). In contrast, our analysis revealed that less than ~5% of *Drd2*- or HA-positive neurons were found to be *Penk*- (**Figure 5a-b**) or FOXP2-expressing cells (**Figure 5c-d**).

The caudal GPe also contains a substantial number of cholinergic neurons which represent 5% of GPe neurons (1,36,37). We therefore assessed the degree of co-localization of *Drd2* or HA-labeled cells with *Slc18a3* and *Chat* encoding the vesicular acetylcholine transporter (VAChT) and the choline acetyltransferase, respectively (**Figure 6**). Our smFISH analysis revealed that *Drd2* positive neurons of the ventro-posterior GPe co-expressed *Slc18a3* (~38%) and *Chat* (~26%) (**Figure 6a-b, e-f**), an observation confirmed by immunofluorescence using VACHT and ChAT antibodies (**Figure 6c-d, g-h**). Altogether, our results indicate that in the caudal GPe, D2R are preferentially expressed by PV/NKX2.1 neurons and to a lesser extent by cholinergic neurons.

Discussion

Since their development more than a decade ago, Drd2$^{eGFP/+}$ or Drd2$^{Cre/+}$ mice crossed with mouse reporter lines expressing any other fluorescent proteins (eGFP, tdTomato) or epitope-tagged proteins (Ribotag) allow mapping the distribution of D2R-expressing cells throughout various brain areas with great precision. If such tools allowed refining the anatomical distribution and cellular composition of D2R neurons within striatum (32,38), it also largely contributed to map the distribution of D2R-expressing cells in brain areas where D2R promotor activity is low such as the hippocampus (25,39,40), cerebral cortex (29,41) or cerebellum (42). By using such approaches and analyzing the distribution of HA-immunoreactive cells in Drd2$^{Cre/+}$;Ribotag$^{f/+}$ mice (25), we found that GPe D2R neurons comprise pallidostriatal, pallidonigral and pallidocortical neurons preferentially localized in the caudal portion of GPe. Our molecular and electrophysiological characterization also unveiled that GPe D2R neurons fall into two distinct neuronal populations, the GABAergic PV/NKX2.1 neurons and cholinergic neurons.

The detection of low density *Drd2* mRNA throughout the GPe was first evidenced by *in situ* hybridization studies performed in rats (21,43-45). While a widespread expression has been initially reported in the rat (21), mouse GPe *Drd2*-expressing cells are mainly detected in the ventro-posterior part as revealed by the expression pattern of HA-positive cells throughout the anteroposterior GPe axis in Drd2$^{Cre/+}$;Ribotag$^{f/+}$ mice. The analysis of mCherry-labeled axons of Drd2$^{Cre/+}$;Ribotag$^{f/+}$ mice injected with AAV2/1. CAGGS.flex.ChR2.tdTomato.SV40 in the caudal GPe allowed us to determine that GPe D2R neurons comprise pallidostriatal, pallidonigral, pallidocortical but not pallidosubthalamic neurons. These data are reminiscent to those obtained with previous anterograde tracing studies performed in rats (36,46). Interestingly, similar to the TS (47), caudal GPe neurons are highly connected with brain areas

involved in visuomotor and auditory processing suggesting that caudal GPe neurons may preferentially regulate sensory-related information.

The vast majority of GPe neurons are GABAergic projection neurons displaying an important level of molecular and functional heterogeneity (3,4,48-51). Among the distinct classes of GPe neurons, *Drd2*/HA-positive neurons strongly co-express markers of GPe prototypic neurons (*Pvalb*/PV and NKX2.1) but lack those identifying GPe arkipallidal neurons (*Penk* and FOXP2) (1). This latter observation contrasts with previous results obtained in rats, in which *Drd2* mRNA expression partially overlap with GPe *Penk*-positive neurons (21) suggesting that the distribution and molecular identity might not be strictly conserved between mice and rats. Such differences might also explain why the increased number of cFos-positive cells detected in the rat GPe following the activation or blockade of D2R (30,52,53) was not observed in mice (**Supplemental Figure 4**).

In addition to be a useful marker of GPe prototypic neurons, NKX2.1 also allows the identification of cholinergic neurons which mainly located in the caudal GPe (1,37,54). Our analysis unveiling that ventro-posterior GPe *Drd2*/HA neurons co-expressed *Slc18a3*/VAChT and *Chat*/ChAT indicate that in addition to be expressing in GPe prototypic neurons, *Drd2*/D2R are also present in a fraction of GPe cholinergic neurons. Interestingly, our electrophysiological recordings also revealed two distinct neuronal populations according to cluster analysis. Type I caudal GPe neurons were characterized by hyperpolarization activated cation currents (Ih), higher spontaneous and maximal firing rates which is reminiscent of the features of GABAergic PV/NKX2.1 neurons (4,34,50). Conversely, type II GPe neurons had lower spontaneous and maximal firing rates and almost no Ih current which is consistent with the electrophysiological profile of cholinergic neurons (34). Finally, our results are in line with the previous tract-tracing

studies indicating that caudal GPe PV neurons largely project to the TS, PIL, SNr pars lateralis but not the STN (46) while caudal GPe ChAT neurons innervate the auditory cortices (36).

Among the basal ganglia nuclei, the GPe is the one displaying the highest density of glial cells comprising namely astrocytes (55). Interestingly, recent studies indicate that dopamine regulates GPe astrocytes functions. Thus, application of quinpirole reduces GPe astrocytic spontaneous Ca^{2+} transients through a mechanism requiring the activation D3R but not D2R (55). Moreover, D2R activation has been shown to regulate the activity of the glial transporter (GAT-3) facilitating GABA uptake by GPe astrocytes (56). Finally, although recent evidence unveil the presence of functional D2R in GPe astrocytes (57), the lack of detection of GFAP/HA-positive cells in the GPe suggest that, if any, basal D2R expression in GPe astrocytes is low.

In conclusion, our work provides the first spatiomolecular characterization of D2R expressing cells in the mouse GPe. Future work will be necessary to disentangle the functional role of D2R within the GABAergic PV/NKX2.1 and cholinergic neurons of the caudal GPe.

Figure Legends

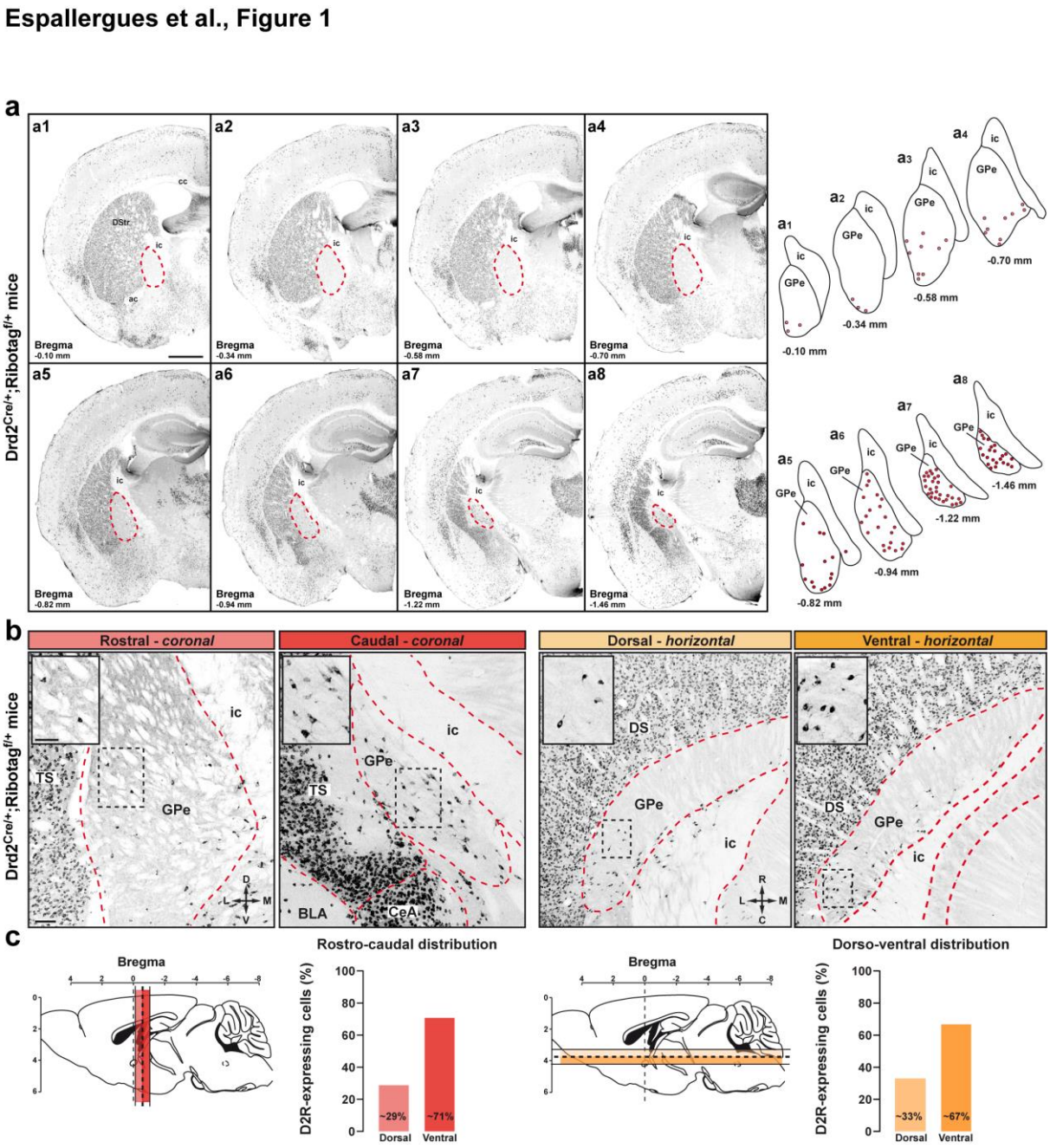

Figure 1. Distribution of D2R cells in the GPe D2-RiboTag mice. a, Coronal GPe sections from Drd2$^{Cre/+}$;Ribotag$^{f/+}$ mice (n = 4) stained with HA. Representative distribution of HA-positive neurons across 8 coronal sections spanning throughout the rostro-caudal axis of the GPe (each dot representing a single neuron). Scale bar: 500 µm. **b**, Representative HA immunolabeled images showing the rostro-caudal (left) and dorso-ventral (right) distributions of HA-positive neurons in the GPe. Scale bar: 100 µm. Inserts are high magnification images

of areas delineated by the black stippled rectangle. Scale bar: 50 μm. **c**, Histograms showing the % HA-positive cells in the GPe throughout the rostro-caudal (left) and dorso-ventral (right) axis. Note the spatial distribution of D2R neurons is biased displaying a highest density in the ventro-posterior GPe. DS: dorsal striatum; TS: tail of the striatum; GPe: external globus pallidus; CeA: central amygdala; BLA: basolateral amygdala; ic: internal capsule; ac: anterior commissure.

Espallergues et al., Figure 2

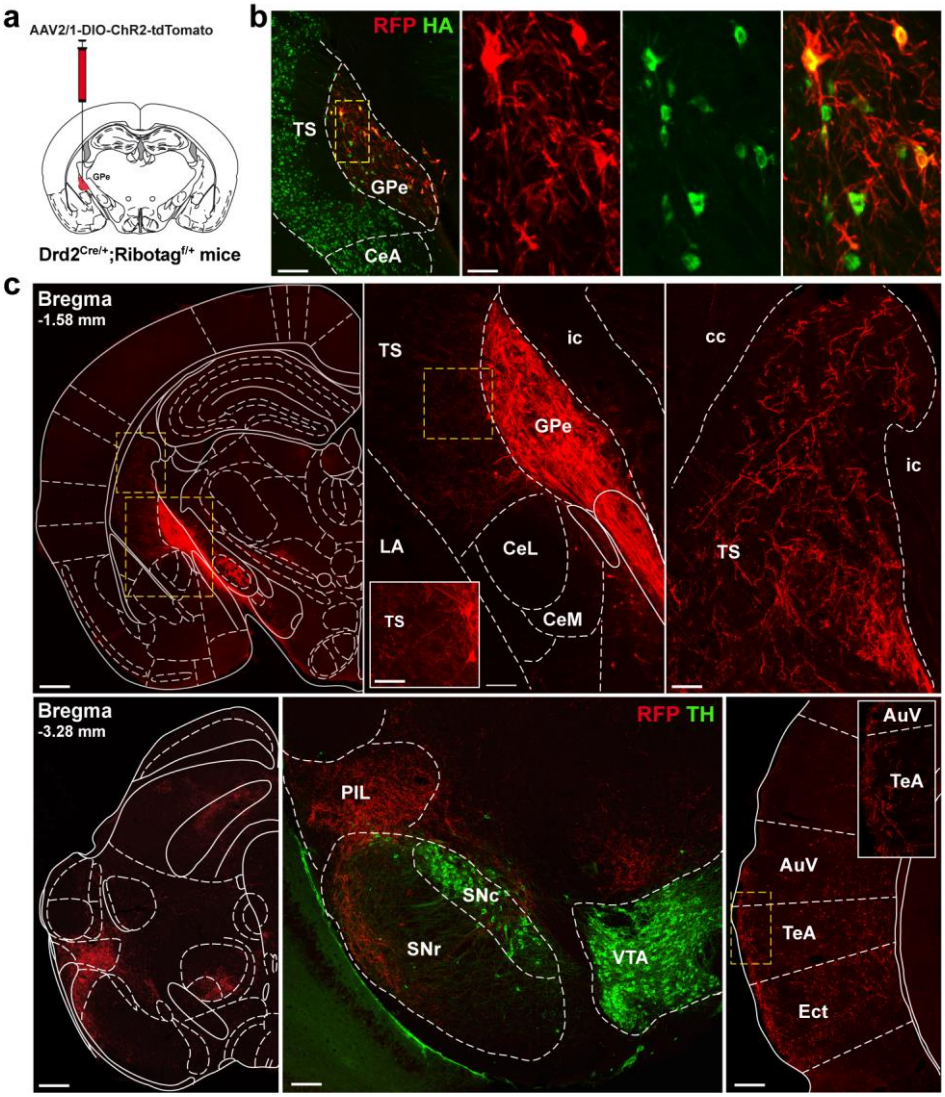

Figure 2. Identification of ventro-posterior GPe D2R neurons projecting areas. a, Schematic representation of the site for the AAV2/1. CAGGS.flex.ChR2.tdTomato.SV40 injection into the caudal GPe of Drd2$^{Cre/+}$;Ribotag$^{f/+}$ mice. **b**, Visualization of ChR2-expressing neurons in the GPe in D2-Ribotag mice. Double immunofluorescence for mCherry (RFP) and HA (green). Scale bar: 70 µm. High magnification image of the area delineated by the yellow stippled rectangle. Scale bar: 20 µm. **c**, Illustration of axon projection targets of ventro-posterior GPe D2R neurons. Note the clear identification of the pallidostriatal, pallidonigral and pallidocortical neurons. Immufluorescence for tyrosine hydroxylase (TH, green) was used to identified SNc and VTA dopamine neurones. TS: tail of the striatum; GPe: external globus

pallidus; CeA: central amygdala; CeL: lateral part of the central amygdala; CeM: medial part of the central amygdala; BLA: basolateral amygdala; LA: lateral amygdala; PIL: posterior intralaminar nucleus; SNr: SN *pars reticulata*; SNc: SN *pars compacta*; VTA: ventral tegmental area; AuV: secondary auditory cortex, ventral area; TeA: temporal association cortex; Ect: ectorhinal association cortex; ic: internal capsule; cc: corpus callosum;

Espallergues et al., Figure 3

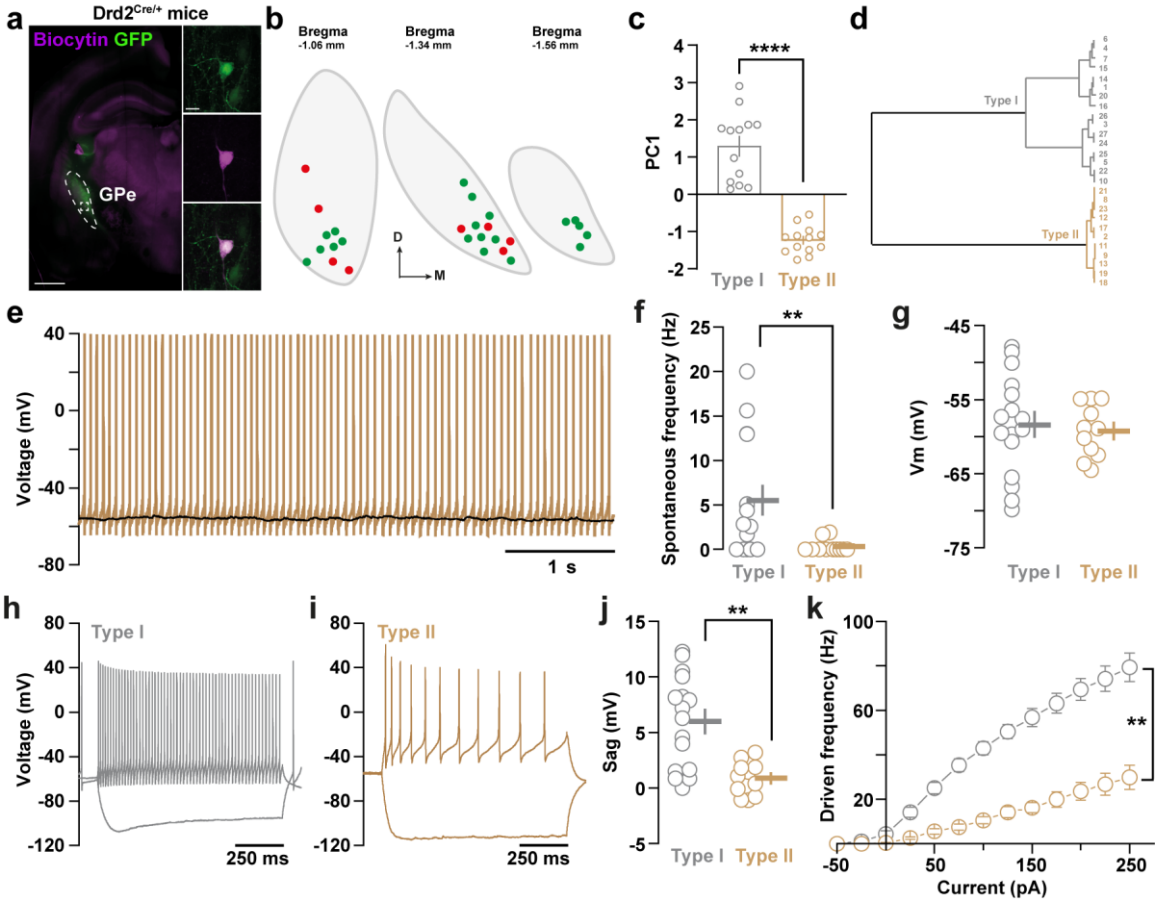

Figure 3. Electrophysiological signature of D2R-expressing neurons located in the ventro-posterior portion of the GPe. a, Low magnification epifluorescent image of a coronal 300-µm thick section showing eYFP-expressing (green) and a biocytin-filled (magenta) GPe neurons. Insets on the left display the biocytin-filled D2R-positive GPe neuron at higher magnification. Scale bar: 10 µm. **b**, Distribution on the rostro-caudal axis of the recorded cells. Green and red dots correspond to recordings performed in $Drd2^{Cre/+}$;AAV-DIO-eYFP (n = 4 mice) and in $Drd2^{Cre/+}$;$Ai9^{f/+}$ mice (n = 6 mice) mice, respectively. **c**, Graph showing the existence of two distinct neuronal populations by principal component analysis. **d**, dendrogram of two main D2R-expressing GPe neuron populations based on their electrophysiological properties. **e**, Representative voltage trace of type II GPe neurons. **f-g**, Graphs depicting spontaneous firing rate (**f**) and resting membrane potential (Vm) (**g**) of type I and type II GPe

neurons. **h-i**, representative traces of voltage response to current step injection (-100 and +100 pA) for a type I (**h**) and a type II (**i**) GPe neuron. **j**, Graph representing the sag value between type I and type II GPe neurons. **k**, Frequency-current (F-i) curve showing the range of firing frequency of type I and type II GPe neurons.

Espallergues et al., Figure 4

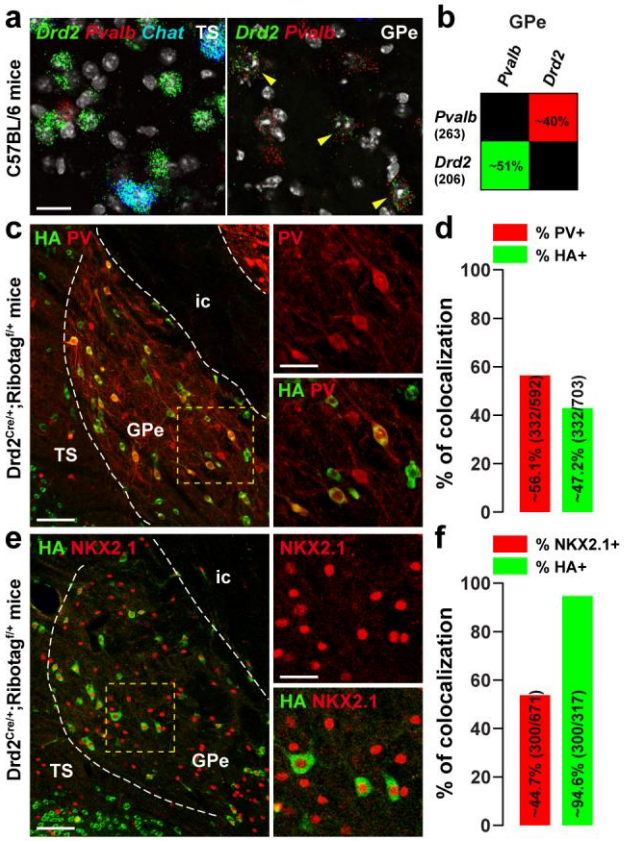

Figure 4. Distribution of *Drd2* among GPe PV and NKX2.1 neurons. a, High magnification of confocal images of coronal brain section of the dorsal striatum (DS, left) and external globus pallidus (GPe, right) from C57BL/6 mouse (n = 3 mice) showing the distribution of *Drd2* (green), *Pvalb* (red) and *Chat* (blue, only for the DS) expression detected with single-molecular fluorescent *in situ* hybridization. Yellow arrows identified *Drd2*/*Pvalb* positive neurons. Slides were counterstained with DAPI (white). Scale bar: 10 µm. **b**, Quantification of the overlap between neurons co-expressing *Drd2*, and *Pvalb* in the ventro-posterior GPe. Values in parentheses indicate the number of neurons identified for each marker (n = 3 mice). Percentages of co-labelling are represented in matrix with probes in columns among neurons labeled with probes in rows (~51% of *Drd2*-positive neurons were also *Pvalb* positive. **c**, **e** Double immunofluorescence for HA (green) and parvalbumin (red, PV) (**c**) and NKX2.1 (red) (**e**) in the caudal GPe of $Drd2^{Cre/+}$;$Ribotag^{f/+}$ mice (n = 6 mice). Scale bar: 50 µm. High magnification

images of areas delineated by the yellow stippled squares. Scale bar: 20 μm. **d**, **f** Histograms showing the co-expression as percentage of HA-labeled neurons (green, HA^+) and as percentage of cells expressing PV (red, PV^+) (**d**) and NKX2.1 (red, $NKX2.1^+$) (**f**). Numbers of HA^+, PV^+ and $NKX2.1^+$ cells counted are indicated in parentheses. TS: tail of the striatum; GPe: external globus pallidus; ic: internal capsule.

Espallergues et al., Figure 5

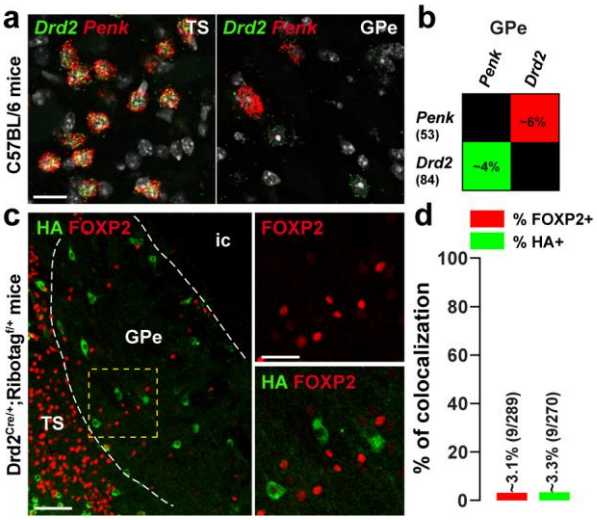

Figure 5. Distribution of *Drd2* among GPe *Penk* and FOXP2 neurons. a, High magnification of confocal images of coronal brain section of the dorsal striatum (DS) and external globus pallidus (GPe) from C57BL/6 mouse (n = 3 mice) showing the distribution of *Drd2* (green) and *Penk* (red) expression detected with single-molecular fluorescent *in situ* hybridization. Slides were counterstained with DAPI (white). Scale bar: 10 μm. **b**, Quantification of the overlap between neurons co-expressing *Drd2* and *Penk* in the ventro-posterior GPe as described in Figure 2b. **c**, Double immunofluorescence (right panels) for HA (green) and FOXP2 (red) in the caudal GPe of $Drd2^{Cre/+}$;$Ribotag^{f/+}$ mice (n = 6 mice). Scale bar: 50 μm. High magnification images of areas delineated by the yellow stippled squares. Scale bar: 20 μm. **d**, Histograms showing the co-expression as percentage of HA-labeled neurons (green, HA^+) and as percentage of cells expressing FOXP2 (red, $FOXP2^+$). Numbers of HA^+ and $FOXP2^+$ cells counted are indicated in parentheses. TS: tail of the striatum; GPe: external globus pallidus; ic: internal capsule.

Espallergues et al., Figure 6

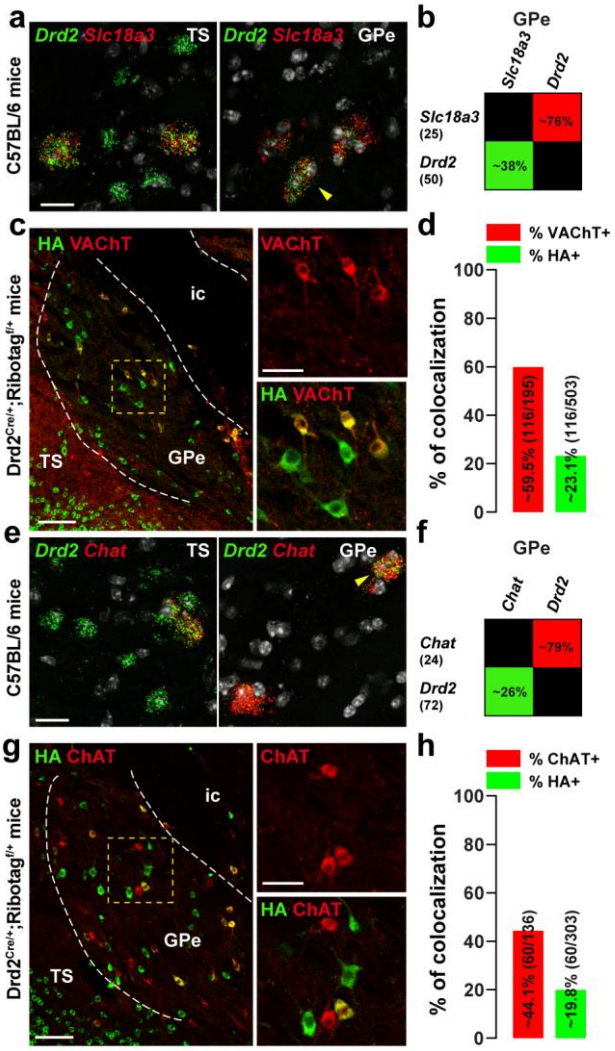

Figure 6. Distribution of D2R among GPe cholinergic neurons. a, **e** High magnification of confocal images of coronal brain section of the dorsal striatum (DS) and external globus pallidus (GPe) from C57BL/6 mouse (n = 3 mice) showing the distribution of *Drd2* (green), *Slc18a3* (red) (**a**) and *Chat* (red) (**e**) expression detected with single-molecular fluorescent *in situ* hybridization. Yellow arrows identified *Drd2*/*Slc18a3* and *Drd2*/*Chat* positive neurons in the DS and GPe. Slides were counterstained with DAPI (white). Scale bar: 10 µm. **b**, **f** Quantification of the overlap between neurons co-expressing *Drd2* and *Slc18a3* (**b**) or *Chat* (**f**) in the ventro-posterior GPe as described in Figure 2b. **c**, **g** Double immunofluorescence (right

panels) for HA (green), VAChT (red) (**c**) and ChAT (red) (**g**) in the caudal GPe of $Drd2^{Cre/+}$;$Ribotag^{f/+}$ mice (n = 5 mice). Scale bar: 50 μm. High magnification images of areas delineated by the yellow stippled squares. Scale bar: 30 μm. **d**, **h** Histograms showing the co-expression as percentage of HA-labeled neurons (green, HA^+) and as percentage of cells expressing VAChT (red, $VAChT^+$) (**d**) or ChAT (red, $ChAT^+$) (**h**). Numbers of HA^+, $VAChT^+$ and $ChAT^+$ cells counted are indicated in parentheses. TS: tail of the striatum; GPe: external globus pallidus; ic: internal capsule.

Funding and Disclosure

This work was supported by Inserm, Fondation pour la Recherche Médicale (EQU202203014705), Agence National de la Recherche (DISCOMMODE, ANR-21-CE37-0013; FrontoFat, ANR-20-CE14-0020; ANR SubDOPA, ANR-21-CE16-0028) (E.V.). JE was a recipient of a postdoctoral fellowship from UM1. The authors declare no conflict of interest.

References

1. Hegeman, D.J., Hong, E.S., Hernández, V.M., and Chan, C.S. (2016). The external globus pallidus: progress and perspectives. Eur. J. Neurosci. *43*, 1239–1265. 10.1111/ejn.13196.

2. Dong, J., Hawes, S., Wu, J., Le, W., and Cai, H. (2021). Connectivity and Functionality of the Globus Pallidus Externa Under Normal Conditions and Parkinson's Disease. Front. Neural Circuits *15*, 645287. 10.3389/fncir.2021.645287.

3. Dodson, P.D., Larvin, J.T., Duffell, J.M., Garas, F.N., Doig, N.M., Kessaris, N., Duguid, I.C., Bogacz, R., Butt, S.J.B., and Magill, P.J. (2015). Distinct developmental origins manifest in the specialized encoding of movement by adult neurons of the external globus pallidus. Neuron *86*, 501–513. 10.1016/j.neuron.2015.03.007.

4. Abdi, A., Mallet, N., Mohamed, F.Y., Sharott, A., Dodson, P.D., Nakamura, K.C., Suri, S., Avery, S.V., Larvin, J.T., Garas, F.N., et al. (2015). Prototypic and arkypallidal neurons in the dopamine-intact external globus pallidus. J. Neurosci. Off. J. Soc. Neurosci. *35*, 6667–6688. 10.1523/JNEUROSCI.4662-14.2015.

5. Aristieta, A., Barresi, M., Azizpour Lindi, S., Barrière, G., Courtand, G., de la Crompe, B., Guilhemsang, L., Gauthier, S., Fioramonti, S., Baufreton, J., et al. (2021). A Disynaptic Circuit in the Globus Pallidus Controls Locomotion Inhibition. Curr. Biol. CB *31*, 707-721.e7. 10.1016/j.cub.2020.11.019.

6. Sadek, A.R., Magill, P.J., and Bolam, J.P. (2007). A single-cell analysis of intrinsic connectivity in the rat globus pallidus. J. Neurosci. Off. J. Soc. Neurosci. *27*, 6352–6362. 10.1523/JNEUROSCI.0953-07.2007.

7. Miguelez, C., Morin, S., Martinez, A., Goillandeau, M., Bezard, E., Bioulac, B., and Baufreton, J. (2012). Altered pallido-pallidal synaptic transmission leads to aberrant firing of globus pallidus neurons in a rat model of Parkinson's disease. J. Physiol. *590*, 5861–5875. 10.1113/jphysiol.2012.241331.

8. Rommelfanger, K.S., and Wichmann, T. (2010). Extrastriatal dopaminergic circuits of the Basal Ganglia. Front. Neuroanat. *4*, 139. 10.3389/fnana.2010.00139.

9. Mamad, O., Delaville, C., Benjelloun, W., and Benazzouz, A. (2015). Dopaminergic control of the globus pallidus through activation of D2 receptors and its impact on the electrical activity of subthalamic nucleus and substantia nigra reticulata neurons. PloS One *10*, e0119152. 10.1371/journal.pone.0119152.

10. Meszaros, J., Cheung, T., Erler, M.M., Kang, U.J., Sames, D., Kellendonk, C., and Sulzer, D. (2018). Evoked transients of pH-sensitive fluorescent false neurotransmitter reveal dopamine hot spots in the globus pallidus. eLife *7*, e42383. 10.7554/eLife.42383.

11. Lindvall, O., and Björklund, A. (1979). Dopaminergic innervation of the globus pallidus by collaterals from the nigrostriatal pathway. Brain Res. *172*, 169–173. 10.1016/0006-8993(79)90907-7.

12. Gauthier, J., Parent, M., Lévesque, M., and Parent, A. (1999). The axonal arborization of single nigrostriatal neurons in rats. Brain Res. *834*, 228–232. 10.1016/s0006-8993(99)01573-5.

13. Aransay, A., Rodríguez-López, C., García-Amado, M., Clascá, F., and Prensa, L. (2015). Long-range projection neurons of the mouse ventral tegmental area: a single-cell axon tracing analysis. Front. Neuroanat. *9*, 59. 10.3389/fnana.2015.00059.

14. Hauber, W., and Fuchs, H. (2000). Dopamine release in the rat globus pallidus characterised by in vivo microdialysis. Behav. Brain Res. *111*, 39–44. 10.1016/s0166-4328(99)00197-7.

15. Napier, T.C., Simson, P.E., and Givens, B.S. (1991). Dopamine electrophysiology of ventral pallidal/substantia innominata neurons: comparison with the dorsal globus pallidus. J. Pharmacol. Exp. Ther. *258*, 249–262.

16. Querejeta, E., Delgado, A., Valdiosera, R., Erlij, D., and Aceves, J. (2001). Intrapallidal D2 dopamine receptors control globus pallidus neuron activity in the rat. Neurosci. Lett. *300*, 79–82. 10.1016/s0304-3940(01)01550-6.

17. Hooper, K.C., Banks, D.A., Stordahl, L.J., White, I.M., and Rebec, G.V. (1997). Quinpirole inhibits striatal and excites pallidal neurons in freely moving rats. Neurosci. Lett. *237*, 69–72. 10.1016/s0304-3940(97)00812-4.

18. Levey, A.I., Hersch, S.M., Rye, D.B., Sunahara, R.K., Niznik, H.B., Kitt, C.A., Price, D.L., Maggio, R., Brann, M.R., and Ciliax, B.J. (1993). Localization of D1 and D2 dopamine receptors in brain with subtype-specific antibodies. Proc. Natl. Acad. Sci. U. S. A. *90*, 8861–8865. 10.1073/pnas.90.19.8861.

19. Yung, K.K., Bolam, J.P., Smith, A.D., Hersch, S.M., Ciliax, B.J., and Levey, A.I. (1995). Immunocytochemical localization of D1 and D2 dopamine receptors in the basal ganglia of the rat: light and electron microscopy. Neuroscience *65*, 709–730. 10.1016/0306-4522(94)00536-e.

20. Khan, Z.U., Gutiérrez, A., Martín, R., Peñafiel, A., Rivera, A., and De La Calle, A. (1998). Differential regional and cellular distribution of dopamine D2-like receptors: an immunocytochemical study of subtype-specific antibodies in rat and human brain. J. Comp. Neurol. *402*, 353–371. 10.1002/(sici)1096-9861(19981221)402:3<353::aid-cne5>3.0.co;2-4.

21. Hoover, B.R., and Marshall, J.F. (2004). Molecular, chemical, and anatomical characterization of globus pallidus dopamine D2 receptor mRNA-containing neurons. Synap. N. Y. N *52*, 100–113. 10.1002/syn.20007.

22. Puighermanal, E., Castell, L., Esteve-Codina, A., Melser, S., Kaganovsky, K., Zussy, C., Boubaker-Vitre, J., Gut, M., Rialle, S., Kellendonk, C., et al. (2020). Functional and molecular heterogeneity of D2R neurons along dorsal ventral axis in the striatum. Nat. Commun. *11*, 1957. 10.1038/s41467-020-15716-9.

23. Gangarossa, G., Perroy, J., and Valjent, E. (2013). Combinatorial topography and cell-type specific regulation of the ERK pathway by dopaminergic agonists in the mouse striatum. Brain Struct. Funct. *218*, 405–419. 10.1007/s00429-012-0405-6.

24. Bertran-Gonzalez, J., Håkansson, K., Borgkvist, A., Irinopoulou, T., Brami-Cherrier, K., Usiello, A., Greengard, P., Hervé, D., Girault, J.-A., Valjent, E., et al. (2009). Histone H3 phosphorylation is under the opposite tonic control of dopamine D2 and adenosine A2A receptors in striatopallidal neurons. Neuropsychopharmacol. Off. Publ. Am. Coll. Neuropsychopharmacol. *34*, 1710–1720. 10.1038/npp.2008.228.

25. Puighermanal, E., Biever, A., Espallergues, J., Gangarossa, G., De Bundel, D., and Valjent, E. (2015). drd2-cre:ribotag mouse line unravels the possible diversity of dopamine d2 receptor-expressing cells of the dorsal mouse hippocampus. Hippocampus *25*, 858–875. 10.1002/hipo.22408.

26. Biever, A., Puighermanal, E., Nishi, A., David, A., Panciatici, C., Longueville, S., Xirodimas, D., Gangarossa, G., Meyuhas, O., Hervé, D., et al. (2015). PKA-dependent phosphorylation of ribosomal protein S6 does not correlate with translation efficiency in striatonigral and striatopallidal medium-sized spiny neurons. J. Neurosci. Off. J. Soc. Neurosci. *35*, 4113–4130. 10.1523/JNEUROSCI.3288-14.2015.

27. Franklin, K.B.J., and Paxinos, G. (2008). The mouse brain in stereotaxic coordinates Compact 3. ed. (Elsevier Academic Press).

28. Cutando, L., Puighermanal, E., Castell, L., Tarot, P., Bertaso, F., Bonnavion, P., de Kerchove d'Exaerde, A., Isingrini, E., Galante, M., Dallerac, G., et al. (2021). Regulation of GluA1 phosphorylation by d-amphetamine and methylphenidate in the cerebellum. Addict. Biol. *26*, e12995. 10.1111/adb.12995.

29. Cousineau, J., Lescouzères, L., Taupignon, A., Delgado-Zabalza, L., Valjent, E., Baufreton, J., and Le Bon-Jégo, M. (2020). Dopamine D2-Like Receptors Modulate Intrinsic Properties and Synaptic Transmission of Parvalbumin Interneurons in the Mouse Primary Motor Cortex. eNeuro *7*, ENEURO.0081-20.2020. 10.1523/ENEURO.0081-20.2020.

30. Marshall, J.F., Henry, B.L., Billings, L.M., and Hoover, B.R. (2001). The role of the globus pallidus D2 subfamily of dopamine receptors in pallidal immediate early gene expression. Neuroscience *105*, 365–378. 10.1016/s0306-4522(01)00180-4.

31. Bertran-Gonzalez, J., Bosch, C., Maroteaux, M., Matamales, M., Hervé, D., Valjent, E., and Girault, J.-A. (2008). Opposing patterns of signaling activation in dopamine D1 and D2 receptor-expressing striatal neurons in response to cocaine and haloperidol. J. Neurosci. Off. J. Soc. Neurosci. *28*, 5671–5685. 10.1523/JNEUROSCI.1039-08.2008.

32. Matamales, M., Bertran-Gonzalez, J., Salomon, L., Degos, B., Deniau, J.-M., Valjent, E., Hervé, D., and Girault, J.-A. (2009). Striatal medium-sized spiny neurons: identification by nuclear staining and study of neuronal subpopulations in BAC transgenic mice. PloS One *4*, e4770. 10.1371/journal.pone.0004770.

33. Sanz, E., Yang, L., Su, T., Morris, D.R., McKnight, G.S., and Amieux, P.S. (2009). Cell-type-specific isolation of ribosome-associated mRNA from complex tissues. Proc. Natl. Acad. Sci. U. S. A. *106*, 13939–13944. 10.1073/pnas.0907143106.

34. Saunders, A., Oldenburg, I.A., Berezovskii, V.K., Johnson, C.A., Kingery, N.D., Elliott, H.L., Xie, T., Gerfen, C.R., and Sabatini, B.L. (2015). A direct GABAergic output from the basal ganglia to frontal cortex. Nature *521*, 85–89. 10.1038/nature14179.

35. Rajakumar, N., Elisevich, K., and Flumerfelt, B.A. (1994). Parvalbumin-containing GABAergic neurons in the basal ganglia output system of the rat. J. Comp. Neurol. *350*, 324–336. 10.1002/cne.903500214.

36. Moriizumi, T., and Hattori, T. (1992). Separate neuronal populations of the rat globus pallidus projecting to the subthalamic nucleus, auditory cortex and pedunculopontine tegmental area. Neuroscience *46*, 701–710. 10.1016/0306-4522(92)90156-v.

37. Nóbrega-Pereira, S., Gelman, D., Bartolini, G., Pla, R., Pierani, A., and Marín, O. (2010). Origin and molecular specification of globus pallidus neurons. J. Neurosci. Off. J. Soc. Neurosci. *30*, 2824–2834. 10.1523/JNEUROSCI.4023-09.2010.

38. Gangarossa, G., Castell, L., Castro, L., Tarot, P., Veyrunes, F., Vincent, P., Bertaso, F., and Valjent, E. (2019). Contrasting patterns of ERK activation in the tail of the striatum in response to aversive and rewarding signals. J. Neurochem. *151*, 204–226. 10.1111/jnc.14804.

39. Rocchetti, J., Isingrini, E., Dal Bo, G., Sagheby, S., Menegaux, A., Tronche, F., Levesque, D., Moquin, L., Gratton, A., Wong, T.P., et al. (2015). Presynaptic D2 dopamine receptors control long-term depression expression and memory processes in the temporal hippocampus. Biol. Psychiatry *77*, 513–525. 10.1016/j.biopsych.2014.03.013.

40. Wei, X., Ma, T., Cheng, Y., Huang, C.C.Y., Wang, X., Lu, J., and Wang, J. (2018). Dopamine D1 or D2 receptor-expressing neurons in the central nervous system. Addict. Biol. *23*, 569–584. 10.1111/adb.12512.

41. Khlghatyan, J., Quintana, C., Parent, M., and Beaulieu, J.-M. (2019). High Sensitivity Mapping of Cortical Dopamine D2 Receptor Expressing Neurons. Cereb. Cortex N. Y. N 1991 *29*, 3813–3827. 10.1093/cercor/bhy261.

42. Cutando, L., Puighermanal, E., Castell, L., Tarot, P., Belle, M., Bertaso, F., Arango-Lievano, M., Ango, F., Rubinstein, M., Quintana, A., et al. (2022). Cerebellar dopamine D2 receptors regulate social behaviors. Nat. Neurosci. *25*, 900–911. 10.1038/s41593-022-01092-8.

43. Bouthenet, M.L., Martres, M.P., Sales, N., and Schwartz, J.C. (1987). A detailed mapping of dopamine D-2 receptors in rat central nervous system by autoradiography with [125I]iodosulpride. Neuroscience *20*, 117–155. 10.1016/0306-4522(87)90008-x.

44. Bouthenet, M.L., Souil, E., Martres, M.P., Sokoloff, P., Giros, B., and Schwartz, J.C. (1991). Localization of dopamine D3 receptor mRNA in the rat brain using in situ hybridization histochemistry: comparison with dopamine D2 receptor mRNA. Brain Res. *564*, 203–219. 10.1016/0006-8993(91)91456-b.

45. Meador-Woodruff, J.H., Mansour, A., Bunzow, J.R., Van Tol, H.H., Watson, S.J., and Civelli, O. (1989). Distribution of D2 dopamine receptor mRNA in rat brain. Proc. Natl. Acad. Sci. U. S. A. *86*, 7625–7628. 10.1073/pnas.86.19.7625.

46. Shammah-Lagnado, S.J., Alheid, G.F., and Heimer, L. (1996). Efferent connections of the caudal part of the globus pallidus in the rat. J. Comp. Neurol. *376*, 489–507. 10.1002/(SICI)1096-9861(19961216)376:3<489::AID-CNE10>3.0.CO;2-H.

47. Valjent, E., and Gangarossa, G. (2021). The Tail of the Striatum: From Anatomy to Connectivity and Function. Trends Neurosci. *44*, 203–214. 10.1016/j.tins.2020.10.016.

48. Mastro, K.J., Bouchard, R.S., Holt, H.A.K., and Gittis, A.H. (2014). Transgenic mouse lines subdivide external segment of the globus pallidus (GPe) neurons and reveal distinct GPe output pathways. J. Neurosci. Off. J. Soc. Neurosci. *34*, 2087–2099. 10.1523/JNEUROSCI.4646-13.2014.

49. Hernández, V.M., Hegeman, D.J., Cui, Q., Kelver, D.A., Fiske, M.P., Glajch, K.E., Pitt, J.E., Huang, T.Y., Justice, N.J., and Chan, C.S. (2015). Parvalbumin+ Neurons and Npas1+ Neurons Are Distinct Neuron Classes in the Mouse External Globus Pallidus. J. Neurosci. Off. J. Soc. Neurosci. *35*, 11830–11847. 10.1523/JNEUROSCI.4672-14.2015.

50. Abrahao, K.P., and Lovinger, D.M. (2018). Classification of GABAergic neuron subtypes from the globus pallidus using wild-type and transgenic mice. J. Physiol. *596*, 4219–4235. 10.1113/JP276079.

51. Pamukcu, A., Cui, Q., Xenias, H.S., Berceau, B.L., Augustine, E.C., Fan, I., Chalasani, S., Hantman, A.W., Lerner, T.N., Boca, S.M., et al. (2020). Parvalbumin+ and Npas1+ Pallidal Neurons Have Distinct Circuit Topology and Function. J. Neurosci. Off. J. Soc. Neurosci. *40*, 7855–7876. 10.1523/JNEUROSCI.0361-20.2020.

52. Ruskin, D.N., and Marshall, J.F. (1997). Differing influences of dopamine agonists and antagonists on Fos expression in identified populations of globus pallidus neurons. Neuroscience *81*, 79–92. 10.1016/s0306-4522(97)00113-9.

53. Billings, L.M., and Marshall, J.F. (2003). D2 antagonist-induced c-fos in an identified subpopulation of globus pallidus neurons by a direct intrapallidal action. Brain Res. *964*, 237–243. 10.1016/s0006-8993(02)04060-x.

54. Rodrigo, J., Fernández, P., Bentura, M.L., de Velasco, J.M., Serrano, J., Uttenthal, O., and Martínez-Murillo, R. (1998). Distribution of catecholaminergic afferent fibres in the rat globus pallidus and their relations with cholinergic neurons. J. Chem. Neuroanat. *15*, 1–20. 10.1016/s0891-0618(98)00016-7.

55. Cui, Q., Pitt, J.E., Pamukcu, A., Poulin, J.-F., Mabrouk, O.S., Fiske, M.P., Fan, I.B., Augustine, E.C., Young, K.A., Kennedy, R.T., et al. (2016). Blunted mGluR Activation Disinhibits Striatopallidal Transmission in Parkinsonian Mice. Cell Rep. *17*, 2431–2444. 10.1016/j.celrep.2016.10.087.

56. Chazalon, M., Paredes-Rodriguez, E., Morin, S., Martinez, A., Cristóvão-Ferreira, S., Vaz, S., Sebastiao, A., Panatier, A., Boué-Grabot, E., Miguelez, C., et al. (2018). GAT-3 Dysfunction Generates Tonic Inhibition in External Globus Pallidus Neurons in Parkinsonian Rodents. Cell Rep. *23*, 1678–1690. 10.1016/j.celrep.2018.04.014.

57. Mastrogiacomo, R., Trigilio, G., Dautan, D., Devroye, C., Ferretti, V., Vitali, E., Orso, G., Marotta, R., Maltese, F., Piras, G., et al. (2021). Astrocytic Regulation of Basal Ganglia Dopamine/D2-Dependent Behaviors (Neuroscience) 10.1101/2021.05.11.443394.

Acknowledgments

The authors thank the iExplore and MRI Platforms of the IGF for their involvement in the maintenance and breeding of the colonies and imaging facilities.

Author contribution

J.E and E.V conceived and led the project. J.E performed stereotaxic injections. J.E, J.B-V and E.V performed immunofluorescence analysis. A.M and M.A performed *in situ* hybridization analysis. M.L-J and J.B performed electrophysiological recordings and related analyses. E.V supervised the project. E.V wrote the manuscript with input from all authors. The authors declare no conflicts of interest.